

# Self-Similarity and Helical Symmetry of Various Vortex Wakes

**Kabardin, I. K. ; Mikkelsen, R. F.; Naumov, I.V.; Okulov, V. L.; Sørensen, J. N.; Velte, C. M.**

*Publication date:*
2018

*Document Version*
Peer reviewed version

# Self-Similarity and Helical Symmetry of Various Vortex Wakes

I.K. Kabardin[1,a)], R.F. Mikkelsen[2], I.V. Naumov[1], V.L. Okulov[2], J.N. Sørensen[2], C.M. Velte[2]

[1]*Kutateladze Institute of Thermophysics SB RAS, Lavrentyev ave. 1, 630090, Novosibirsk, Russia.*
[2]*Technical University of Denmark, 2800, Lyngby, Denmark*

[a)] Corresponding author: kabardin@itp.nsc.ru

**Abstract.** The present work examines the local structure and downstream evolution of both longitudinal vortexes behind the vortex generators and the helical tip vortices generated by the rotating 3-bladed rotor. Both wakes flow with the strong longitudinal or helical vortices have been studied by stereo PIV measurements in a wind tunnel or a water flume accordingly. The vorticity field was calculated from the measured velocity fields. The downstream development of vortex local cores investigates by using self-similarity scaling arguments and local helical symmetry tests simultaneously. It was analyzed Batchelor's vortex and 2-D vortex with a helical vortex to use a combined vortex model of the helical self-similarly for a comparison with the experimental data. The experimental study of the shape of both vortices was carried out to describe the downstream development of the expanding vortex core by the new combined vortex model based on the experimental observations triggered by previous studies of wakes behind vortex generators and rotors. It was established that the local helical symmetry with a simple correspondence between the axial and azimuthal velocity in the cores exists in all cross-sections along of both longitudinal and helical vortices. It is also found that the averaged vorticity profiles inside the core of both vortices are self-similar. This knowledge is important for the fundamental understanding of the vortex flows, as well as for the aspect of applications, for which parametric descriptions can be substantially reduced in terms of required time and cost by easing engineering models.

## INTRODUCTION

The present work examines the local structure and downstream evolution of both longitudinal vortexes behind the vortex generators and the helical tip vortices generated by the rotating 3-bladed rotor (Fig. 1). These vortices were the subject of many theoretical, experimental and numerical investigations [1]. For example, in [2-3] the problem of the stability of a helical vortex system was considered analytically. In [4,5] embedded vortices in turbulent wall-bounded flow over a flat plate, generated by a vortex generator with variable angle β to the incoming flow have been studied. The self-similarity of velocity and vorticity was found. In numerical studies [6], the self-similarity of vorticity and azimuthal velocity profiles were indicated too.

## MODELING OF THE VORTEX

Batchelor [7] proposed a correlation between space and time in the diffusion solution (see Lamb–Oseen vortex e.g. [6]) replacing time $t$ by a spatial parameter $x/B$

$$\Delta r_c^2 \equiv r_c^2(z) - r_c^2(z_0) = 4(z - z_0)\nu_k / B$$

where $B = U_0$ is an incoming flow. In his vortex, the azimuthal and axial velocity components take the forms:

$$ru_\theta(z,r) = C_0\left(1-e^{-\eta}\right),\quad u_z(z,r) = B - De^{-\eta}/8\pi\, z\nu_k\,, \tag{1}$$

where $\eta = Br^2/4z\nu_k$ , and the constant $C_0 \equiv \Gamma/2\pi$ represents $1/2\pi$ times the flow circulation, and $D$ describes the "drag" of the body divided by density $\rho$ .

Flows with helical vorticity also can be characterized by the velocity field [9]:

$$u_z = u_0 - \frac{\Gamma}{2\pi l}\left(1-\exp\left(-\frac{r^2}{\varepsilon^2}\right)\right),\quad u_z + ru_\theta / l = u_0 \tag{2}$$

where $u_0$ is the advection velocity of the vortex; $l=H/2\pi$ is the pitch of the helical vortex lines; $\Gamma$ is the vortex strength (circulation) and $\varepsilon$ is the effective size of the vortex core with Gaussian axial vorticity distribution. The simple model (2) keeps constant to the vortex core size $\varepsilon$. The self-similar expansion of the vortex core (1) and the solution including helical symmetry (2) could be collected as the new combined vortex model in a form

$$u_\theta = \frac{\Gamma}{2\pi r}\left[1-\exp\left(-\frac{r^2}{r_c^2(z)}\right)\right],\ u_z = B - \frac{\Gamma}{2\pi l(z)}\left[1-\exp\left(-\frac{r^2}{r_c^2(z)}\right)\right]\,, \tag{3}$$

The model (3) only requires empirical functions or experimental calibration of some few flow parameters: vortex circulation - $\Gamma$, helical pitch - $l$, advection velocity along vortex axis – $B$, and growth factor of the vortex core - $r_c$.depending from the azial distance $z$. All mentioned parameters will be determined experimentally by using PIV measurements of the velocity field in the next section.

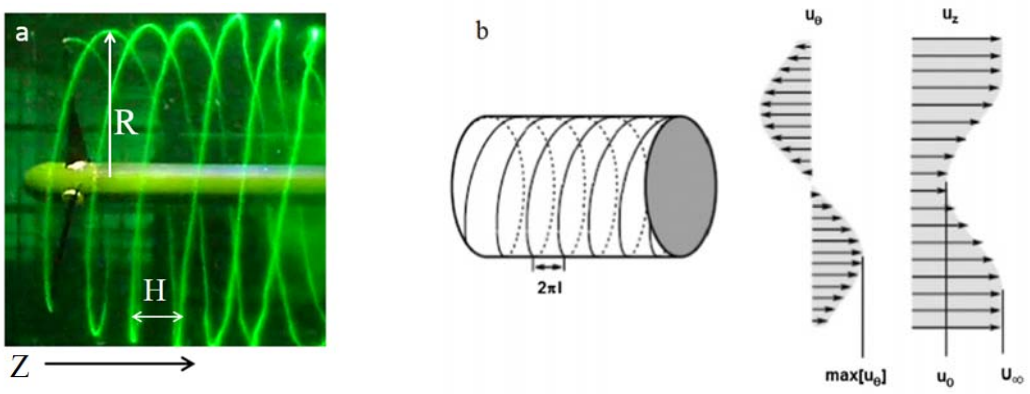


**FIGURE 1.** Visualization of tip vortices behind rotor (a) [10] and a principal sketch of helical vortex and self-similarity normalization parameters (b) [5].

## EXPERIMENTAL SETUP AND METHOD

The investigations with vortex generators were carried out in a low-speed closed-circuit wind tunnel recording Stereoscopic Particle Image Velocimetry (SPIV) velocity fields in cross planes at free-stream speed $U_\infty$ = 1 m/s(figure 2). The rectangular vortex generators, positioned directly on the flat test section wall, were the same height as the boundary-layer thickness, $h = \delta$ = 25 mm, and with a length of $L = 2h$ = 50 mm [5]. The SPIV system was mounted on a traverse so that the equipment could be moved in the stream-wise direction to measure the development in several positions without requiring re-calibration. For each measurement position, 500 independent realizations were acquired.

A self-similarity investigation in rotor wake was made with the model of three-bladed rotor specially manufactured for qualitative and quantitative flow visualizations downstream of the rotor [10]. The rotor diameter was 2R = 0.376 m, and the length of the blade was 0.159 m with the CD7003 blade profile. The blade chord and angle of attack along span were calculated with the optimal tip speed ratio (TSR) $\lambda$ = 5, where $\lambda = \Omega R/V$, and $\Omega$ is the angular speed of the rotor. The Reynolds number was about 200 000 at the working temperature of 20º C in the water flume. The water flume had a length of 35 m, a width of 3 m and the operative height was 0.9 m. A 3-m long

test section with transparent walls of the optical resolution was installed at a distance of 20 m from the channel inlet; the test section walls and bottom were made of glass.

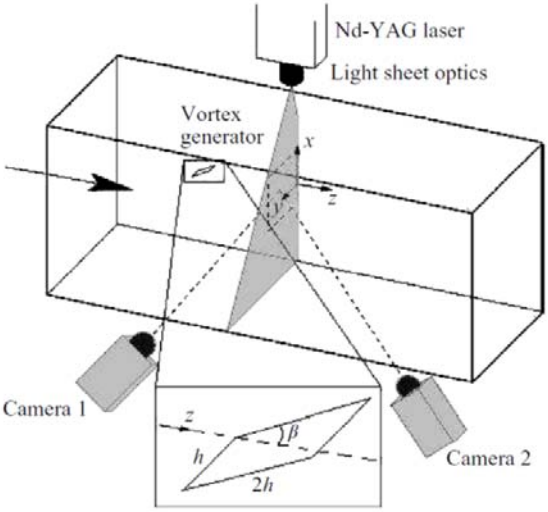


**FIGURE 2.** Schematic illustration of the experimental set-up and device geometry for rectangular vortex generator. The large arrow to the left indicates the main flow direction and β the device angle. The measurement plane in the laser sheet has been indicated by dashed lines [5].

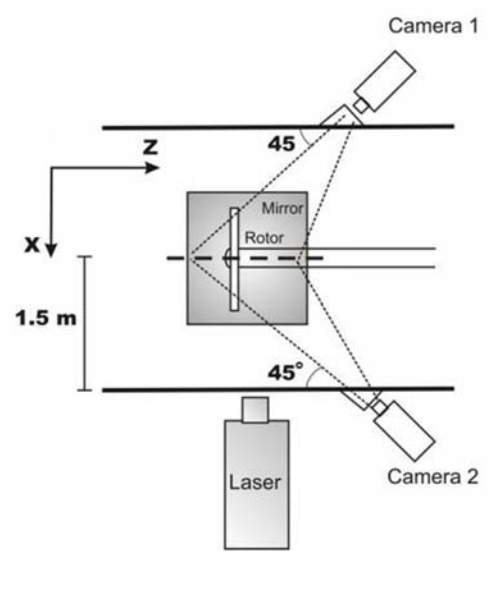


**FIGURE 3.** Sketch of PIV measurements in both cross-sections of the flume and directions of the global coordinates [10].

The flow behind the rotor was studied by the Dantec Stereoscopic 2D-3C PIV system which gives all three velocity components throughout widow of the light sheet. An Nd:YAG laser was used as a light source with the following characteristics: 120 mJ of energy in a single pulse, the wavelength is 532 nm. The light sheet was sent in vertically into the channel from the bottom and directly aiming at the rotor axis. The images were recorded by two Dantec HiSense II cameras with 1344 ÷ 1024 pixels resolution. The cameras were placed perpendicularly to each other on the different sides of the flume and at an angle of 45º to the walls (Figure 3). Water-filled optical prisms were installed between the cameras and the test section to reduce the distortions having from the camera inclination to the wall. The measuring error of stereoscopic PIV was at the level of 3÷5 %. The final size of the total 3D velocity field was 1.03·0.29 m. For each measuring window, the ultimate velocity field was obtained by phase averaging of 100 realizations, which were recorded in the moment of a triggered signal by a light pulse per the one revolution of the rotor.

## RESULTS

For vortex generators, the averaged flow fields were recorded in cross planes to give a full view of the vortex at each position. Figure 4 shows the axial ($u_z$) and azimuthal ($u_\theta$) velocity profiles at four angles $\beta$ =0 degree. The figure 3 shows $u_z$ and $u_\theta$ for each downstream position, while the mid and right columns show $u_z$ and $u_\theta$, respectively, with the applied self-similarity scaling. As it seen the self-similarity takes place. For some downstream positions, asymmetry occurs on the left side. This is mainly caused by the presence of the wall, perturbing the velocity field of the vortex core [5]. Figure 5 displays the streamwise evolution of the helical parameters $u_0$, $\Gamma$, $l$ and $\varepsilon$, where the last two were averaged over $\theta$ Up to about 1–2 vane heights downstream of the generator. Further downstream (at about 13 vane heights) perturbations in the secondary velocities due to the neighboring vortices become too large, and the model can no longer be applied. The velocity formulation Eq. (1-4) comprises, in addition to the axial and azimuthal velocity profiles, the convection velocity $u_0$ and the helical pitch $l$. Since both velocity profiles are self-similar, both $u_0$ and $l$ are expected to vary linearly along the downstream direction, which is confirmed by Figure 5. The negative sign of $l$ indicates that the helical vortex has a left-handed symmetry [9]. The coupling to ε is far more complex, but the vortex core is expected to expand due to viscous diffusion. The only

parameter that is not expected to vary is the circulation, which should always be close to constant in a system of low-viscous dissipation (figure 5).

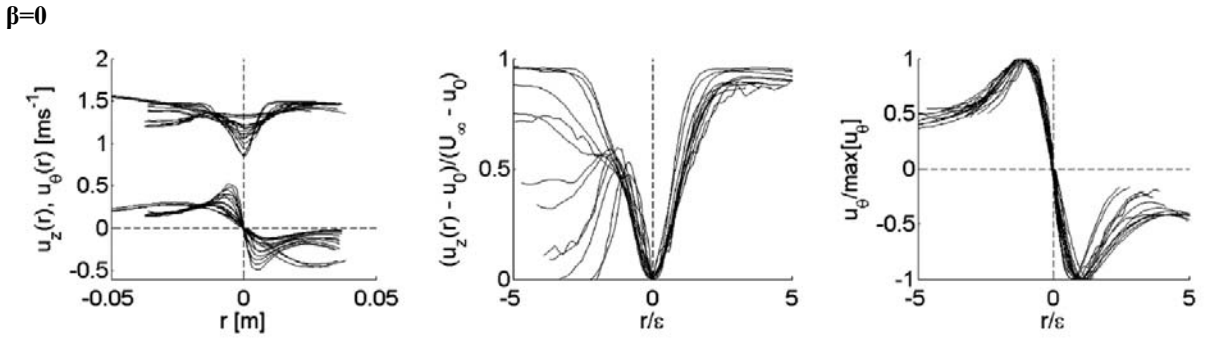


**FIGURE. 4.** Axial ($u_z$) and azimuthal ($u_\theta$) velocity profiles (left) and the axial (middle) and azimuthal (right) ones scaled by self-similarity variables [5].

For the rotor wake the distributions of the components of the axial, radial and transverse velocity were measured in the different planes of the laser knife and also the vorticity field was calculated from the measured velocity fields. The cross-sections of the tip vortex cores are well fixed which make it possible to determine the centers of the tip vortices in the cross-sections. The regular vortex structure destroyed for coordinate $z$ between 1.8 R to 3.6 R and pairing with nearest turns takes place behind 3 R. If each cross-section of tip vortex cores is numbered from 1 to 9, then the vortex cores No. 1, 4, 7 correspond to the first blade, cores No. 2, 5, 8 correspond to the second blade, and cores No. 3, 6, 7 correspond to the third blade. Diffusion of tip vortices is taken place.

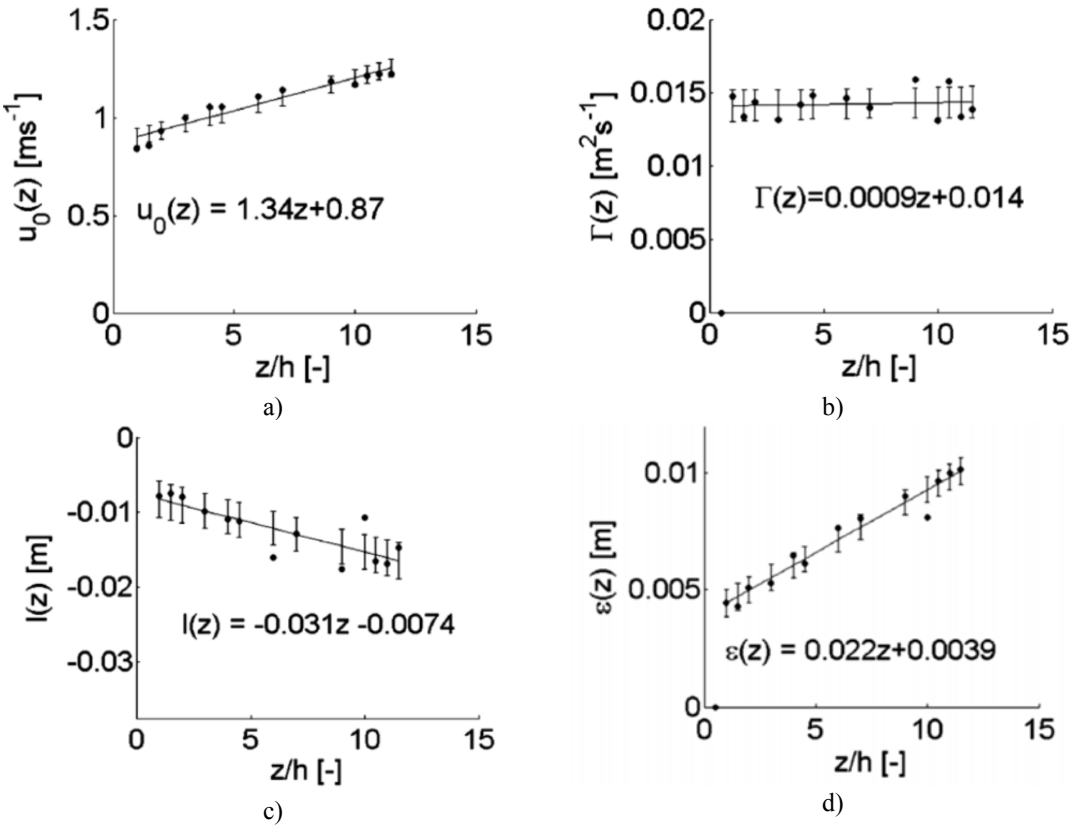

**FIGURE 5.** Downstream evolution of the characteristic vortex parameters in the stable wake of vortex generator [5].

The averaging is allowed by the linear correlation between the two velocities in (5). In accordance to this, in the following azimuthally averaged local velocities and vorticity will be used:

$$\omega_z(z,r)=\frac{1}{2\pi}\int_0^{2\pi}\omega_z(z,r,\theta)d\theta\,,\ u_\theta(x,r)=\frac{1}{2\pi}\int_0^{2\pi}u_\theta(z,r,\theta)d\theta\,,\ \ u_z(z,r)=\frac{1}{2\pi}\int_0^{2\pi}u_z(z,r,\theta)d\theta \qquad (5)$$

The scaling radial similarity variable is for the 1st, 4th, and 7th vortex core determined as the value of the radius $\varepsilon$, where the azimuthal velocity $u_\theta$ takes its maximum. Therefore, the scaled values of the profiles (5) for a fixed axial position $z$ or vortex number, can be recalculated by

$$\tilde{\omega}_z(z,r/\varepsilon(z))=\frac{\omega_z(z,r/\varepsilon(z))}{\max\limits_r[\omega(z,r)]}\,,\ \tilde{u}_\theta(z,r/\varepsilon(z))=\frac{u_\theta(z,r/\varepsilon(z))}{\max\limits_r[u_\theta(z,r)]}\,,\ \tilde{u}_z(z,r/r_c(x))=\frac{u_z(z,r/\varepsilon(z))}{\max\limits_r[u_z(z,r)]} \qquad (6)$$

Examples of axial vorticity profiles at cross-sections 1, 4, 7, corrected from minor asymmetries by azimuthal averaging, are shown in figure 6, a. The same profiles scaled by (6) are shown in figure 6,b and compared to the analytical solution (1). To determine the local velocity distribution in the in the polar plane of the vortex core, the transport velocity of the center of the vortices was measured and subtracted from the total velocity of each cross section. Figure 6,a shows the local azimuthal velocity $u_\theta$ in cross-sections 1, 4, 7 after removal of the transport velocity. The scaling by (1-6) of the profiles clearly indicates the existence of self-similarity of the local azimuthal velocity inside the tip vortex (figure 6, b).

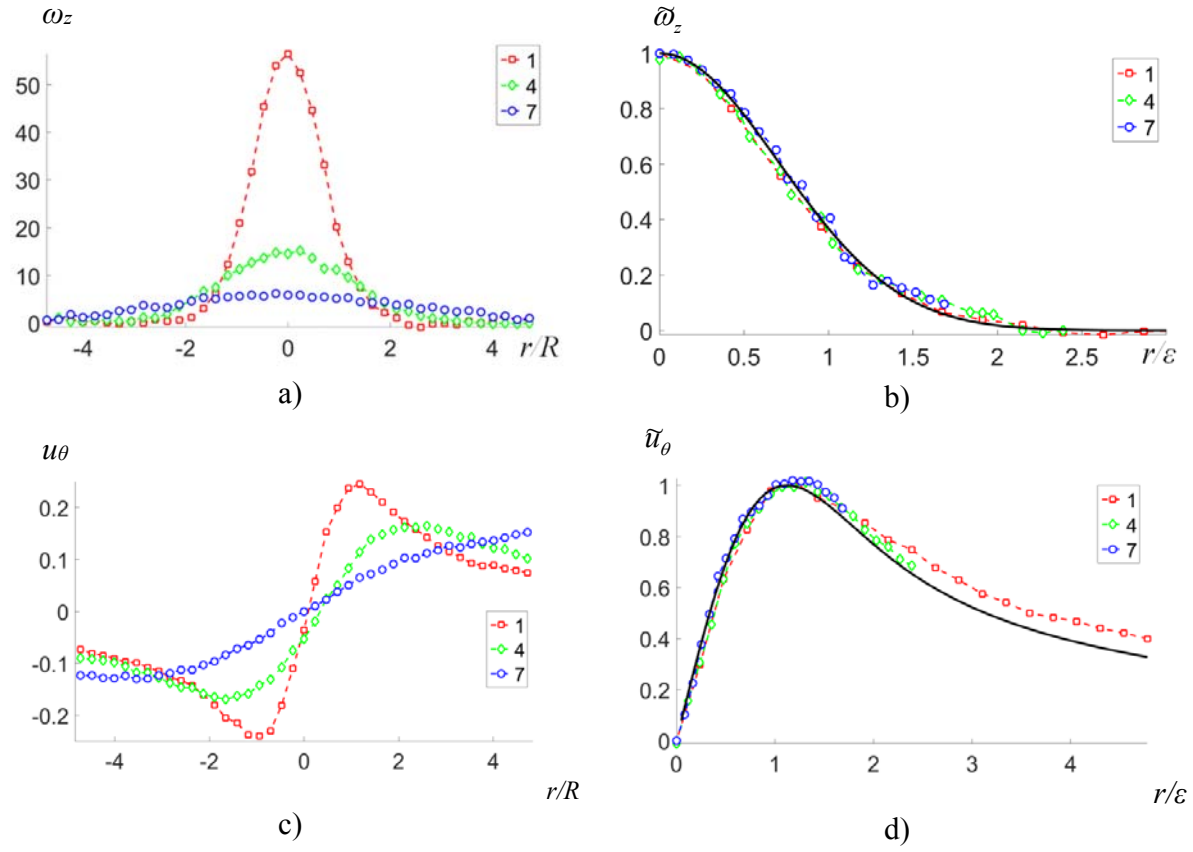

**FIGURE 6.** (a) Lines with the symbols indicate the original PIV profiles of the local vorticity in the core at different cross-sections of the tested helical vortex. (b) Comparison of the same half profiles, scaled by equation (6), with the analytical non-dimensional solution (1) shown by a solid line.(c) Lines with symbols are the original PIV profiles of the local azimuthal velocity in the different cross-sections of the tip helical vortex. (d) The self-similar behavior of the same profiles scaled by equation (6) with the analytical non-dimensional solution (2) shown by a solid line.

The evolution of helical parameters in resented in figure 7. As seen in figure 7, the circulation does not change along the tip vortex (figure7, a). Evolution of vortex core shows expansion presented in fig 7. b. The evolution of helical pitch is presented in figure 7.c.

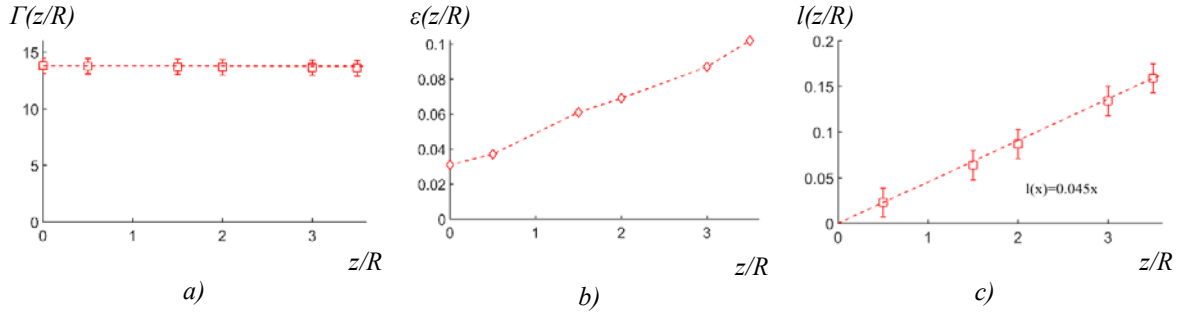


**FIGURE 7.** Downstream distribution of circulation (a) vortex core radius (b) and local helical pitch (c).

The next plot (figure 8, a) shows the local axial velocity extracted directly from the global azimuthal velocity. A small total wake rotation exists due to the hub vortex generated in the center of the rotor wake, which gives rise to a negative overshoot of the local axial velocity profiles (figure 8, a). The linear velocity formulation for local helical symmetry (4) allows the usage of averaged velocity fields (5) to determine the helical vortex characteristics. The good correlation of the velocity profiles (figure 8, b) in accordance with the formula (2) permits to conclude the existence of a local helical structure of the tip vortex core.

As a next step, we transform the original local axial velocity profiles (figure 8, a) into the form $u_d(z,r) = [u(z,r) - u_0(z)]$. This result is shown in figure 8b where the deficit velocity, made dimensionless by $\Gamma/2\pi l$, depends inversely on the axial distance (1/z), as indicated by the self-similar solution (2). The comparisons clearly indicate that the local flow distribution in the tip vortex core is Gaussian and that it exhibits helical self-similarly.

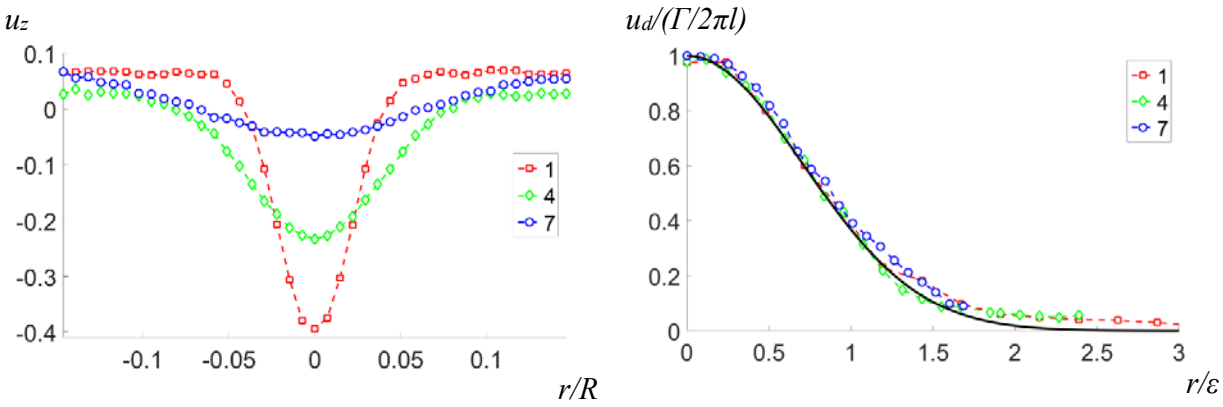


**FIGURE 8.** (a) Lines with symbols are the Original PIV profiles of the local axial velocity in different cross-section of tip vortex (b) The self-similarity behavior of the axial velocity deficit in the tip vortex core scaled by (6).

## CONCLUSION

The vortex generated by a rectangular vortex generator displays self-similar behavior for $z/h \approx 2–13$. This is observed for both the axial and azimuthal velocity profiles, which are linearly related. Consequently, all the characteristic parameters (convection velocity, helical pitch, circulation, and radius) vary linearly along the downstream direction and the radius and pitch are only weakly dependent on the angle $\beta$ [5]. Further, these linear trends in the helical parameters have been observed also for vortex development over adverse pressure gradients. This means that, unless vortex breakdown occurs somewhere along the way, one should be able to interpolate the helical parameters linearly and, thus, model and describe the full vortex flow field. Further, the counter-rotating cascade arrangement of the vanes is seen to reduce the perturbations of neighboring secondary vortices.

Helical tip vortices generated by a three-bladed rotor were measured using stereoscopic PIV measurements in a water flume, with the aim of investigating possible self-similarity of the velocity profiles in the vortex core. The data were analyzed and processed assuming different self-similarity scaling arguments. Both the local azimuthal vorticity profiles and the local axial and azimuthal velocity components were investigated and showed the existence of helical self-similarity, which is well described by the proposed model (1-6). Furthermore, a good correlation existed between measurements and vortex flow decay using Batchelor's vortex (2-3) with a Gaussian vortex core. The proposed self-similarity scaling arguments enable further investigations of e.g. the stability of helical vortex cores, where expressions of full velocity profiles along the vortex axis are required.

The achieved knowledge is important for the fundamental understanding of vortex flows as well as for different practical applications in which the parametric description requires the use of simplified analytical engineering expressions.

## ACKNOWLEDGMENTS

The study was supported by the Russian Science Foundation RSF14-19-00487.

## REFERENCES

1. J.N. Sørensen Instability of helical tip vortices in rotor wakes// Journal of Fluid Mech., 682, 1–4 (2011).
2. V.L. Okulov On the stability of multiple helical vortices// J. Fluid Mech., 521, 319-342 (2004).
3. V.L. Okulov and J.N. Sørensen Stability of helical tip vortices in a rotor far wake//J. Fluid Mech., 576, 1-25(2007).
4. C.M. Velte, M.O. Hansen and V.L. Okulov Helical structure of longitudinal vortices embedded in turbulent wall-bounded flow// J. Fluid Mech., 619, 167-177 (2009).
5. C.M. Velte Vortex Generator Flow Model Based on Self-Similarity // AIAA J., 51(2), 526 – 529 (2013).
6. M. Ali and M. Abid Self-similar behavior of a rotor wake vortex core// J. Fluid Mech. 740, 1–11 (2014).
7. Batchelor G. K. Axial flow in trailing line vortices// J. Fluid Mech. 20, 645–658(1964).
8. P.A. Kuibin and V.L. Okulov One-dimensional solutions for a flow with a helical symmetry// Thermophysics and Aeromechanics, 3(4), 335–339 (1996)
9. S.V. Alekseenko, P.A. Kuibin and V.L. Okulov Theory of concentrated vortices. An introduction (Berlin, Heidelberg, New York: Springer, 2007).
10. V.L. Okulov, I.V. Naumov, R.F. Mikkelsen, I. K. Kabardin and J.N. Sørensen A regular Strouhal number for large-scale instability in the far wake of a rotor// J. Fluid Mech., 747, 369–380 (2014).